Journal of Molecular Liquids 387 (2023) 122597

Contents lists available at ScienceDirect

Journal of Molecular Liquids

journal homepage: www.elsevier.com/locate/molliq

Histidinehydroxamic acid as new biomolecule to produce molecular-like fluorescent gold nanoclusters: Possible mechanisms for metal ion sensing

Gyöngyi Gombár [a], Péter Simon [b], Ditta Ungor [a,c], István Szatmári [b,d], Edit Csapó [a,c,*]

[a] MTA-SZTE Lendület "Momentum" Noble Metal Nanostructures Research Group, University of Szeged, Rerrich B. sqr. 1, H-6720 Szeged, Hungary
[b] Institute of Pharmaceutical Chemistry, University of Szeged, Eötvös u. 6, H-6720 Szeged, Hungary
[c] Interdisciplinary Excellence Center, Department of Physical Chemistry and Materials Science, University of Szeged, Rerrich B. sqr. 1, H-6720 Szeged, Hungary
[d] Stereochemistry Research Group, Eötvös Loránd Research Network, University of Szeged, Eötvös u. 6, H-6720 Szeged, Hungary

ARTICLE INFO

Keywords:
Gold nanoclusters
Fluorescence
Histidine
Hydroxamic acid derivatives
Metal ion sensors

ABSTRACT

We firstly demonstrate a new biomolecule, Histidinehydroxamic acid (HisHA), to produce few-atomic fluorescent gold nanoclusters (Au NCs) in aqueous medium. The preparation protocol has been optimized by studying the effect of metal ion/biomolecule molar ratio, metal ion concentration, pH, temperature, reaction time as well as the role of citrate as mild reducing agent on appearance of blue-emitting (λ_{em} = 440 nm, λ_{ex} = 365 nm) molecular-like NCs. Structural studies confirmed that imidazole-*N* and amino-*N* of the HisHA stabilize the formed metallic cores. The quantum yield of ~ 4% and fluorescence lifetime of 4.2 ns were determined. Moreover, these NCs show suitable stability under high inert salt (c_{NaCl} = 2.5 M) concentration as well. Verifying its ability to detect metal ions, dual strategies were discovered. We confirmed that the copper ions cause fluorescence quenching (LOD = 2.49 μM) by pushing the higher amount of soft HisHA ligand from the metallic surface and forming complexes with dominantly hydroxamate-[O,O] coordination mode in the aqueous medium. For Zn^{2+}-ions, a "turn-on" sensing mechanism was observed; the smallest detectable amount of Zn^{2+} is 7.5 μM. Linear increase of the quantum yield (from ~ 4% to ~ 11.5%) was identified above 75 μM of Zn^{2+} due to the binding of the Zn^{2+}-ions on the cluster surface via hydroxamate-[O,O] donors.

1. Introduction

Gold nanoparticles (Au NPs) and gold nanoclusters (Au NCs) are one of the most widely studied nanostructured materials among the metal-based systems in recent years, due to their outstanding optical, chemical, and physical properties and therefore have an exceedingly wide range of potential application possibilities [1]. The Au NCs have discrete energy levels, which lead to their unique fluorescence, excellent photophysical and chemical stability, and good biocompatibility [2]. The noble metal nanoclusters (NCs) consist of a few or a few tens of metal atoms with a diameter of < 2 nm, thus forming a bridge between metal atoms and NPs. These NCs are formed via a reduction of the precursor ions (*e.g.* $AuCl_4^-$) by assembling individual atoms one by one. The size, as well as the composition of NCs, can be systematically adjusted by the synthesis conditions or by the quality and quantity of the reducing and stabilizing agents. By controlling the size, the composition as well as the type of surface functionalizing ligand(s) these NCs are potent candidates in various applications such as biomedical engineering, bioimaging, medicine, catalysis, metal ion or molecule detection [3]. For biomedical applications, the so-called "green" chemical synthesis methods are strongly preferred [4]. Among the many routes of preparation, the template-assisted method is one of the most commonly used, because the biomolecule serving as the template acts as the reducing, stabilizing and surface-functionalizing molecule [5]. Plant extracts such as tea leaves, various citrus fruits and peppermint are used for this type of synthesis [4]. In addition, biomolecules (amino acids [6], peptides, proteins [3], or nucleotides [7]) are also suitable for the direct reduction of gold ions and the stabilization of Au NCs.

Amino acids are a popular class of reducing agents because they are almost universally present in biological system. Previously, Au NCs have been synthesized via the direct interaction of *L*-histidine (His), *L*-tyrosine (Tyr), *L*-proline (Pro), *L*-tryptophan (Trp) and *L*-methionine (Met) with $[AuCl_4]^-$ which possess intense blue photoluminescence (PL), except Met, where the NCs show yellow emission [6]. For *L*-cysteine the

* Corresponding author at: MTA-SZTE Lendület "Momentum" Noble Metal Nanostructures Research Group, University of Szeged, Rerrich B. sqr. 1, H-6720 Szeged, Hungary.
E-mail address: juhaszne.csapo.edit@med.u-szeged.hu (E. Csapó).

https://doi.org/10.1016/j.molliq.2023.122597
Received 16 May 2023; Received in revised form 12 July 2023; Accepted 13 July 2023
Available online 16 July 2023

formation of a well-known and widely characterized self-assembled coordination polymeric structure is confirmed [8].

Hydroxamic acids are weak acids, *N*-hydroxy amides, and are highly reactive compared to amides, which have high stability. They can be found in two different tautomeric forms, the keto form in acidic media and the iminol form in basic media [9]. The currently known medical applications of hydroxamic acids are based on their outstanding chelating properties (*e.g.* with Fe(III), Zn(II)), but there is no article in the literature on the production of Au NCs using hydroxamic acids. Au NCs have high photostability, which allows their use for sensing purposes, as in most cases the emission intensity of the Au NCs depends on the chemical environment, thus allowing the detection of various metal ions and small molecules [10]. Chelating functional groups on the surface of the clusters can be advantageous for the design of NCs-based metal ion sensors, which was the main motivation for the present research work.

Based on these findings, in this work, we aim to develop a novel synthesis protocol for the preparation of Au NCs using a hydroxamic acid derivative of *L*-histidine (HisHA) amino acid as a template ligand. We studied the reduction capability of this newly applied molecule against $AuCl_4^-$, which has not been reported in the literature earlier. Moreover, the metal ion sensing properties of the HisHA-Au NCs are also studied and compared to the experimental results of the fluorescent nanosized product formed in the pure histidine- $AuCl_4^-$ system (His-Au) [11]. The "turn-off" and "turn-on" fluorescence mechanisms have been identified and interpreted for Cu^{2+} and Zn^{2+}, respectively.

2. Experimental

2.1. Materials

Histidinehydroxamic acid ($C_6H_{10}N_4O_2$, HisHA) was synthesized in our laboratory according to the procedure mentioned below in 2.2. Chapter. Hydrogen tetrachloroaurate (III) monohydrate ($HAuCl_4{\cdot}H_2O$, 99.9% (metal basis)), copper(II) chloride ($CuCl_2$, 97%), zinc(II) chloride ($ZnCl_2$, ≥98%), *L*-Histidine ($C_6H_9N_3O_2$, ≥99%) were obtained from Sigma-Aldrich. Tri-sodium-citrate-2-hydrate ($C_6H_5Na_3O_7{\cdot}2H_2O$, 99%, Na-cit), sodium hydroxide (NaOH, 99%), hydrochloric acid (HCl, 37%), sodium chloride (NaCl, 99.98%) were purchased from Molar. The other tested mono-, di- and trivalent metal salts were in chloride form and their purity was more than 99.0 % and were obtained from Sigma-Aldrich. All the chemical reagents were analytical grade and were used without further purification. The fresh stock solutions were prepared by using Milli-Q ultrapure water (18.2 MΩ·cm at 25 °C) in each case.

2.2. Synthesis of HisHA

The precursor hydroxamic acid derivative HisHA **(2)** was synthesized based on the former literature method [12–14], starting from *L*-histidine methyl ester dihydrochloride (**1**) by implementing different optimization steps: *i)* for the synthesis of the hydrochloride of the corresponding amino acid esters (**1**) was applied; *ii)* the reactions were performed in water by using hydroxylamine solution (50 wt% in H_2O) as a reagent. This latter nucleophilic agent was used in excess, first to *in situ* liberate the hydrochlorides, and secondly to keep the reaction mixture in alkaline medium providing by this an easy work-up procedure *e.g.* the product was crystallized directly from the reaction mixture (Scheme 1).

Namely, 1.0 g (4.13 mmol) of *L*-histidine methyl ester dihydrochloride (**1**) was placed in a round-bottomed flask and dissolved in 10 mL of water. 20 mL of hydroxylamine solution (50 wt% in H_2O) was added, and the reaction mixture was stirred at room temperature. After reaching maximal conversion (24 h reaction time, when the TLC (thin layer chromatography) showed no more starting material) the mixture was cooled down by using an ice bath, and the formed crystals were filtered and washed with cold water (2 × 7 mL). Yield: 440 mg (63 %); M.p.: 176–178 °C; ^{1}H NMR (DMSO-d_6, **Fig.S1**) δ: δ:2.51–2.59 (1H, m); 2.75–2.83 (1H, m); 3.25–3.31 (1H, m); 6.77 (1H, s); 7.50 (1H, s); MS (**Fig.S2**): $[M + H^+]$ m/z = 171.16; $[M + Na]^+$ m/z = 193.17.

2.3. Synthesis of HisHA-stabilized Au NCs

Firstly, 1.497 mL of 0.0167 M HisHA aqueous solution was added to 2.953 mL of Milli-Q water. After stirring for 2 min, 50 μL of Na_3-cit ($c_{citrate}$ = 1 M) and 500 μL of $HAuCl_4$ solution (c_{AuCl4^-} = 10 mM) were also administrated into the reaction mixture. After mixing the components, sample was thermostated at 80 °C ± 1 °C for 48 h under pH = 7.0. According to the concentration of components, HisHA:$AuCl_4^-$/ 5:1 M ratio was used, while the final concentration of the gold was 1.0 mM. The use of citrate promoted the cluster formation; in the sample HisHA/citrate 1:2 M ratio was applied. Combined application of HisHA and citrate is necessary for cluster formation; the citrate alone does not result in NCs at 80 °C, the reaction is shifted toward plasmonic NPs formation. After synthesis, the small aggregates were removed by centrifugation at 13.000 rpm for 30 min, while the final product was purified by dialysis for 180 min using a cellulose dialysis tube with a 1 kDa cut-off. A generally accepted protocol was applied for dialysis in our lab. The specific conductance of the dialysis medium is measured continuously, and the fluorescence of the sample is also registered in parallel. If the fluorescence intensity starts to decrease, presumably the clusters have diffused through the membrane, and the specific conductance of the medium shows an increasing trend, the dialysis is stopped. The dialysis time determined at the intersection of the inflection phase of the two curves is usually adopted as the optimum. For our system this is 180 min.

2.4. Instruments for characterization

The fluorescence spectra of the NCs were recorded on Jobin Yvon Fluoromax-4 spectrofluorometer (Horiba) using excitation wavelength at 365 nm with a 3 nm slit in a 1 cm quartz cuvette. The fluorescence lifetime was measured on a Horiba DeltaFlex device by time-correlated single photon counting (TCSPC) technique. A DeltaDiode pulsed laser (λ_{em} = 371 nm) as an excitation light source and a quartz cuvette with 1 cm optical length was applied for the measurements. The absolute

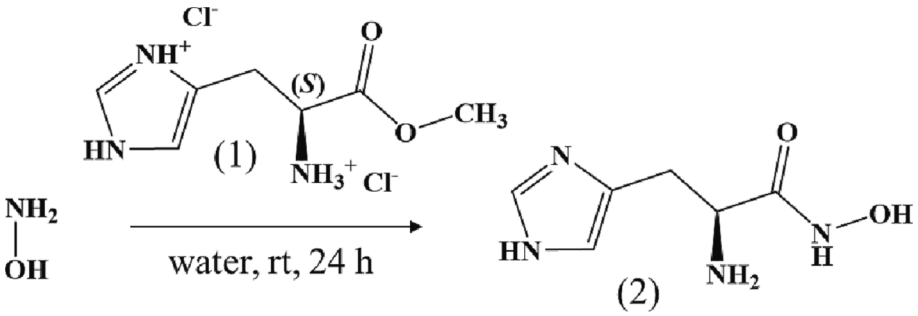

Scheme 1. Synthesis of HisHA **(2)**.

quantum yield was determined in a 1 cm cuvette by an ABL&JASCO FP-8500 spectrofluorometer equipped with an ABL&JASCO ILF-835 integrating sphere. For the calibration of the instrument, a calibrated ABL-JASCO ESC-842 WI lamp was used, therefore another reference was not needed. The UV–Vis spectra were recorded on the ABL&E-JASCO V-770 Spectrophotometer in the range of 300–600 nm using a 1 cm optical path length. Infrared spectra of the pure molecules, as well as the NCs in powder form, were measured by Jasco FT/IR-4700 in the attenuated total reflectance (ATR) mode at room temperature from 3500 cm^{-1} to 700 cm^{-1}. The resolution was 2 cm^{-1} with 256 scans for all the samples. The pH of the samples was kept constant. The ζ-potential measurements were performed at 25.0 ± 0.1 °C using a Malvern NanoZS instrument (λ = 633 nm He-Ne laser).

2.5. Experimental conditions of the sensor studies

The fluorescent histidine-stabilized gold nanohybrid systems (His-Au) were prepared based on a publication published previously by our research group [11] as a reference. For sensing, 500–500 μL of purified His-Au and HisHA-Au NCs were added into 1.100 mL of MQ ultrapure water, and an aqueous solution containing 400 μL of several mono-, di-, and trivalent metal ions were also added to the NCs dispersion, separately, where the concentration of the tested ions was constant (c_{ions} = 1.0 mM). The appropriate ionic strength (c = 1.0 M) was provided by sodium chloride. The emission spectra of the Au NCs were recorded at room temperature both in the absence and in the presence of the added ions. For Cu^{2+} detection, detailed fluorescence quenching studies were performed with a range of Cu^{2+} concentrations (1 nM – 100 mM). For Zn^{2+} detection, the fluorescence spectra of the NCs in the presence of Zn^{2+} ions were registered in the range of 1 nM – 100 mM of Zn^{2+} concentration. Where necessary, the fluorescence spectra were corrected for the corresponding absorbance spectra according to **Eq. (1)**.

$$I_{corr} = I_m \times 10^{(A_{EX}+A_{EM})/2} \quad (1)$$

where I_{corr} is the corrected fluorescence intensity and I_m is the fluorescence intensity measured at 440 nm (HisHA-Au NCs) and 475 nm (His-Au system). A_{ex} and A_{em} are the absorbances measured at the excitation wavelength ($\lambda_{ex\text{-}HisHA\text{-}Au\ NCs}$ = 365 nm; $\lambda_{ex\text{-}His\text{-}Au}$ = 378 nm) and the absorbance measured at the emission wavelength ($\lambda_{em\text{-}HisHA\text{-}Au\ NCs}$ = 440 nm; $\lambda_{em\text{-}His\text{-}Au}$ = 475 nm), respectively. For the evaluation of the data, I_{corr} values are expressed as I.

3. Results and discussion

3.1. Developing of the preparation protocol of HisHA-directed Au NCs

To find the suitable synthesis conditions, thereby producing the final nanosized product with the most intense fluorescence, the syntheses have been carried out at different HisHA:$[AuCl_4]^-$ molar ratios. We investigated the role of the molar ratio in the range of 0.1:1–10:1 HisHA:$[AuCl_4]^-$, where the final concentration of the metal was 1.0 mM. The reaction mixture was thermostated at 80 °C and continuously monitored the appearance of the intense fluorescence of the samples under UV light (for about 24 h). After 24 h, the fluorescence spectra (Fig. 1**A**) were registered by a spectrofluorometer at λ_{ex} = 365 nm.

As Fig. 1**A** shows the appearance of an emission band at λ_{em} = 440 nm, which has increasing intensity by increasing the HisHA:$[AuCl_4]^-$ molar ratio from 0.5:1 to 5:1. The highest fluorescence intensity is observed at HisHA:$[AuCl_4]^-$ /5:1 ratio (Fig. 1**A, inset**). With a further increase in the HisHA excess, the PL intensity starts to decrease. To find other important reaction parameters this HisHA:$[AuCl_4]^-$ / 5:1 molar ratio was kept constant. In a second step, the effect of the pH of the medium in the pH range 1–12 (Fig. 1**B**) was studied considering the deprotonation ability of the ligand [15] as well as the well-known pH-dependent hydrolysis of the $AuCl_4^-$ ions in aqueous solution [16]. It was found that the more alkaline pH range (pH = 7–10) is more preferred for the formation of the nanosized fluorescent product. After 24 h synthesis time the pH of the reaction mixture is pH ~ 7, so this value was chosen for further studies. Previous investigations for His-Au also confirmed that the formation of NCs starts parallel with the deprotonation of the imidazolium moiety (pK_{imid} ~ 6.0) and the acidic condition (pH < 6) is not suitable for NCs production [11]. Three additional parameters (metal concentration (Fig. 2**A**), temperature (Fig. S3**A**), and synthesis time (Fig. S3B)) were also optimized, while keeping the previously defined parameters constant.

The role of the metal ion concentration was investigated in the range 0.1–2.0 mM, and it was obtained that the optimal metal ion concentration is 1.0 mM, because at higher metal ion concentrations lower PL can already be detected and slight aggregation of the NCs is observed. Moreover, the increase in the metal concentration causes the formation of colloidal Au particles. In terms of the temperature, the syntheses were carried out at several temperatures between 25 and 80 °C but lowering the temperature did not have a positive effect on the appearance of

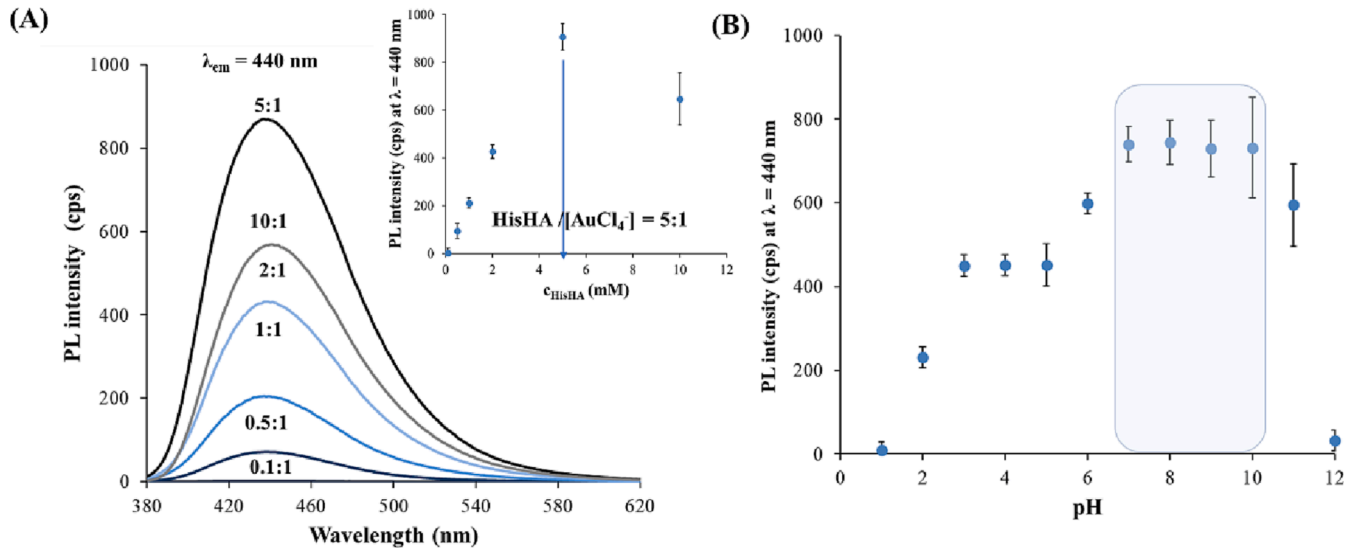

Fig. 1. (A) Fluorescence spectra of the samples after 24 h at different HisHA:$[AuCl_4]^-$ molar ratios with the maximum emission intensities at λ_{em} = 440 nm as a function of c_{HisHA} (inset) (c_{Au} = 1.0 mM, pH = 7.0, λ_{ex} = 365 nm). **(B)** Fluorescence intensities of the emission band at λ_{em} = 440 nm as a function of the pH (c_{Au} = 1.0 mM, HisHA:$[AuCl_4]^-$ /5:1, λ_{ex} = 365 nm).

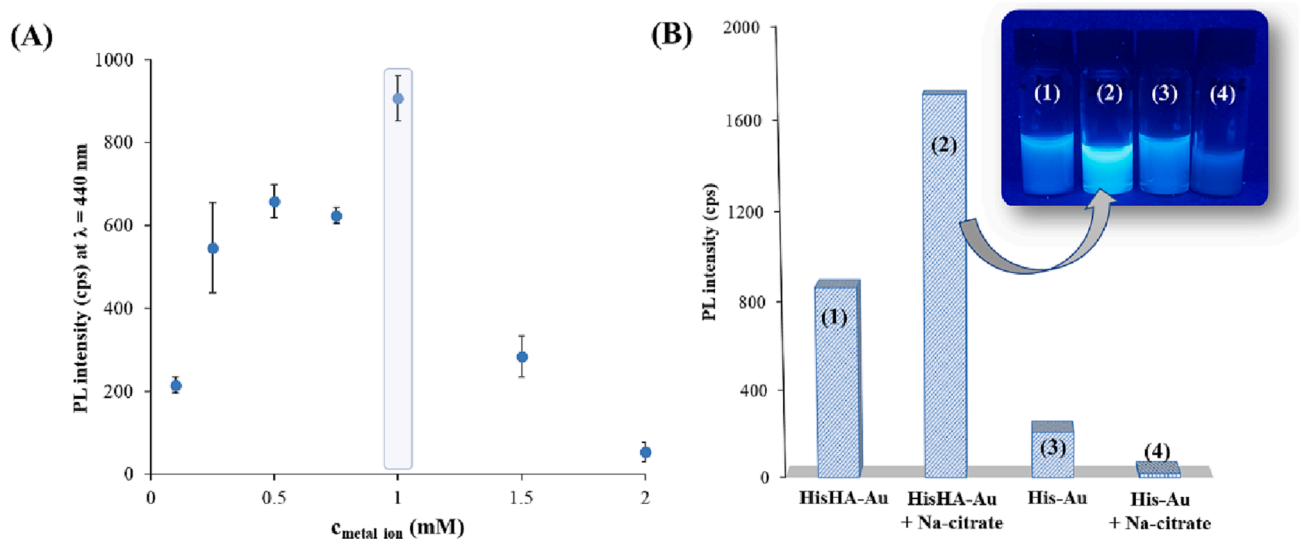

Fig. 2. **(A)** Effect of metal ion concentration in the HisHA-$AuCl_4^-$ sample (HisHA: $AuCl_4^-$/5:1, pH = 7.0, λ_{ex} = 365 nm); **(B)** Fluorescence intensity values of the final products formed in the HisHA-$AuCl_4^-$ and in the His-$AuCl_4^-$ systems in the presence and in the absence of citrate (HisHA:$AuCl_4^-$/5:1, pH = 7.0, λ_{em} = 440 nm, λ_{ex} = 365 nm, His:$AuCl_4^-$/30:1, pH = 6.0, λ_{em} = 475 nm, λ_{ex} = 378 nm, c_{AuCl4-}= 1.0 mM) The SD of the PL measurements is ~ 3%.

fluorescent products, so 80 °C was adopted. For higher temperature (~100 °C) the PL intensity decreases drastically (Fig. S3A), because the formation of NPs, instead of the appearance of fluorescent clusters, will be preferred in the system. As a final step of the synthesis, the synthesis time was optimized. The emission spectra of the samples were registered for a few days, and we observed that the highest intensity can be reached after 48 h, under the constant parameters defined previously. Finally, to facilitate the complete reduction of precursor metal ions as well as to increase the yield of the fluorescent product, the presence of sodium citrate as an auxiliary reducing agent was also investigated. The synthesis was carried out at several citrate concentrations (**Fig.S4**), but it was found that the ideal amount is 10.0 mM (HisHA:Na-citrate/1:2 molar ratio) supporting an increase in the yield of fluorescent gold products. If the amount of sodium citrate is further increased, the PL intensity values show a decreasing trend, because the large amount of ligand can sterically hinder the growth of the cluster cores. We also investigated the role of citrate because, in the pure His amino acid - $[AuCl_4]^-$ system (at pH ~ 6), even under high ligand excess (His:$[AuCl_4]^-$/30:1), the blue-emitting product formed is a helically ordered polynuclear complex with a metal ion oxidation state of + 1 [11]. For comparison of the two systems, the effect of citrate was also studied for His-$AuCl_4^-$ system as well (Fig. 2**B**). As Fig. 2**B** clearly represents hydroxamic acid derivatives of His, the application of citrate as a mild reducing agent is highly beneficial because the fluorescence intensity can be nearly doubled. In contrast, for His-containing samples the presence of citrate has a rather negative effect on the formation of the fluorescence product and the complete reduction of the metal ion does not occur. The photos of the samples under the UV-lamp also support this observation. In conclusion, the incorporation of the hydroxamate group on histidine leads to the formation of nanoclusters rather than complexation under the application of citrate. It is well-known that the citrate alone does not result in the formation of NCs; the appearance of plasmonic NPs occurs via the reduction of gold ions with citrate at high temperature (~100 °C) [17]. It can be concluded that the mixture of HisHA and citrate is more advantageous to produce NCs.

The final product was purified in a two-step procedure since subsequent measurements can be strongly influenced by the presence of unreacted precursor metal salt and electrolyte ions that may remain from the reduction process. In the first step, the dispersion was purified by centrifugation at 13000 rpm for 30 min, followed by dialysis for 180 min at room temperature using a cellulose tube with a cut-off of 1 kDa, using ultrapure Milli-Q water as a dialysis medium. The purity of the clusters produced was checked by measuring the fluorescence signal and the conductivity of the dialysis medium as presented in 2.3 Chapter.

3.2. *Optical and structural characterization of the fluorescent products*

The first step was to determine the comprehensive optical features of the purified nanostructures, including the registration of the optical spectra, the determination of the absolute quantum yield (QY%) and PL lifetime values. The UV–Vis spectra of the newly prepared HisHA-Au NCs and the initial HisHA molecule, as well as the emission spectrum of the prepared NCs, are presented on Fig. 3**A**, while the typical fluorescence decay curve with the distribution of the three main lifetime components is shown on the Fig. 3**B**.

As the registered spectra show, the λ_{ex} = 365 nm can serve as excitation wavelength to reach intensive blue emission (λ_{em} = 440 nm) in the case of HisHA-Au quantum clusters. The utilization of exciting light was analyzed by quantum yield (QY%) measurements, and the fluoresce decay curve was registered by the TCSPC method. The calculated data for HisHA-Au NCs are summarized in Table 1**.** with the same data determined for the fluorescent product formed in the pure histidine – $AuCl_4^-$ system.

As it can be seen, the QY% is a slightly higher value in the case of HisHA-Au NCs, which suggests that the combined use of the hydroxamate derivative of His with the sodium citrate is favorable for the synthesis of fluorescent gold nano-objects. Based on the fittings of the decay curves, three main lifetime components can be identified in both systems. In the case of the His-Au complex, the longer lifetimes clearly refer to the Au(I) complex structure, while the shorter T1, T2 and T3 values decisively refer to the more metallic particularity in the case of the HisHA-Au system. Considering the literature data, the shorter T2 (0.07 ± 0.01 ns) may originates from the π···π stacking of the HisHA [18]. The longer T1 (1.87 ± 0.09 ns) and T3 (4.19 ± 0.06 ns) values belong to the metal-involved emissions, which are the ligand-to-metal (LMCT) and ligand-to-metal–metal charge transfers (LMMCT), respectively [19,20].

For structural characterization, FT-IR studies have also been performed. Infrared spectroscopy is one of the most commonly used analytical methods to identify the structure of a compound and monitor its sub-processes. **Fig.S5** shows the infrared spectra of hydroxamic acid-based NCs before and after the synthesis of metal clusters. For HisHA-

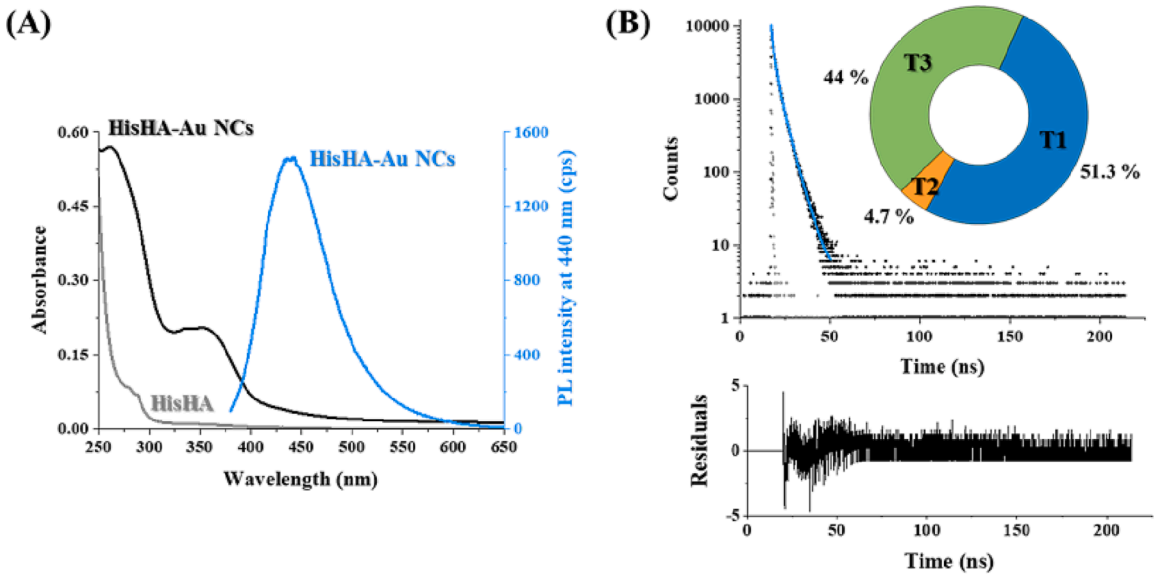

Fig. 3. **(A)** The UV–Vis spectra of the HisHA (grey) and HisHA-Au NCs (black) with the emission spectra of the prepared HisHA-Au NCs (blue) (c_{HisHA} = 3.0 mM; $c_{HisHA\text{-}Au\ NCs}$ = 1.0 mM (calculated on Au concentration), λ_{ex} = 365 nm; λ_{em} = 440 nm). **(B)** The typical fluorescence decay curve of HisHA-Au NCs with the contribution percentage of the main lifetime components (λ_{ex} = 371 nm; λ_{em} = 450 nm).

Table 1
Main data of the optical measurements (λ_{ex}: excitation wavelength, λ_{em}: emission wavelength, **QY%**: average quantum yield % using the defined λ_{ex}, **T1-T2-T3**: main lifetime components). The χ^2 values represent the goodness of fitting.

Sample	λ_{ex} (nm)	λ_{em} (nm)	QY %	T1 (ns)	T2 (ns)	T3 (ns)	χ^2
His-Au CPs [#]	378	475	3.6	0.74	4.03	9.13	1.14
HisHA-Au NCs	365	440	4.2	1.87	0.07	4.20	1.02

[#] CPs = coordination polymeric structure containing Au(I).

based NCs, the intensity of the characteristic vibrations of the imidazole ring (3125 cm^{-1}, 3030 cm^{-1}) is reduced upon interaction with the aurate ions, suggesting that metal coordination is likely to involve these nitrogen atoms and the amino-*NH* bending vibration is also shifted from 1575 cm^{-1} to 1556 cm^{-1} [15]. We cannot perform a detailed structural analysis based on the FT-IR spectrum, because the formation of a metallic surface is supported by the quality (flattening of the characteristic vibration bands) of the IR spectrum. The formation of HisHA-Au NCs is likely due to the extra citrate used in the synthesis and the ionic reaction by I^- ions (the color change was not observed).

3.3. Interaction with different metal ions: Sensor studies

For sensor development in biological systems, it is important to first investigate the salt tolerance of fluorescent products. For this purpose, NaCl with increasing concentration (0.25–2.5 M) was added to the aqueous dispersion of the HisHA-Au NCs. There was no significant change (Fig.S6) in the emission intensity of the clusters, confirming their potential use in biological media. The fluorescence of the clusters is highly sensitive to the chemical environment, so the presence of certain metal ions may affect their fluorescence. The interaction of our HisHA-Au NCs with several mono-, di- and trivalent metal ions having different electronic structures are studied. After the addition of metal ions to the NCs-containing aqueous dispersion the fluorescence signal was recorded. For all these measurements, the same volume of cluster dispersion

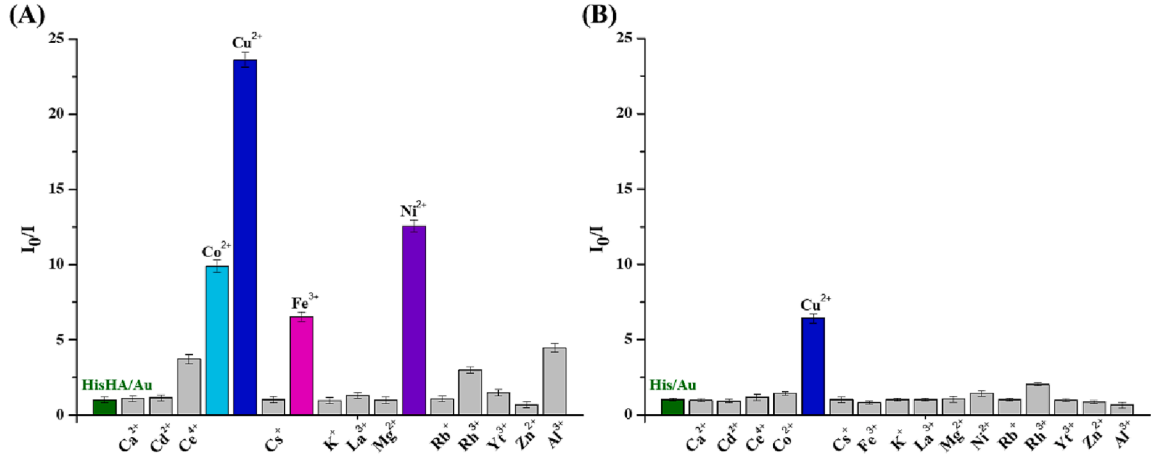

Fig. 4. **(A)** Corrected relative fluorescence of HisHA-Au NCs in presence of different metal ions (c_{Au} = 0.25 mM, $c_{metal\ ions}$ = 1.0 mM, c_{NaCl} = 1.0 M, T = 25 °C, λ_{ex} = 365 nm, λ_{em} = 440 nm). **(B)** Corrected relative fluorescence of His-Au coordination polymeric structure in the presence of different metal ions ($c_{metal\ ions}$ = 1.0 mM, c_{Nacl} = 1 M, T = 25 °C, λ_{ex} = 378 nm, λ_{em} = 475 nm).

was used, and, in each sample, the concentration of the metal ions was also the same (c = 1.0 mM). The results are presented in Fig. 4**.** If there is any interaction between the metal cluster and the metal ions, an enhancement, quenching, or shift in the characteristic fluorescence can be generally observed. As shown in Fig. 4**A**, the fluorescence of HisHA-Au NCs was dominantly quenched by four different metal ions to varying degrees. It was observed that Co^{2+}, Cu^{2+}, Fe^{3+} and Ni^{2+} metal ions cause approximately 10-, 24-, 6- and 13-fold decrease in fluorescence of HisHA-Au NCs. In addition, HisHA-Au NCs show fluorescence enhancement only in the presence of Zn^{2+}-ions ($I_0/I < 1.0$).

As reference the above-mentioned studies were performed for the His-Au system (in this case not NCs present in the system, only Au(I)-containing coordination polymeric structure is confirmed) as well. As Fig. 4**B** shows for His-Au only the Cu^{2+} ions cause a 6-fold decrease in fluorescence which is not significant. We can conclude that the incorporation of the hydroxamic acid group having good chelating properties into the His amino acid facilitates the detection of more metal ions, and in the case of Cu^{2+}, we observed a fluorescence quenching almost four times more efficient than it was found for pure amino His amino acid-based nanohybrid system. Naturally, the fluorescence quenching assays were investigated for HisHA-Au NCs in the absence of Na-citrate for Co^{2+}, Ni^{2+}, Cu^{2+} and Fe^{3+} metal ions as well. As the **Fig.S7** shows, improved I_0/I values were detected in the absence of Na-citrate. This positive effect mainly changes the LOD value of Cu^{2+} significantly. For Cu^{2+} the LOD (in the presence of citrate) = 2.49 μM, LOD (in the absence if citrate) = 1.35 μM. For other 3 metal ions the LOD was not detected again in the absence of citrate, in the presence of citrate these LOD values were varied in the range of ~ 5–10 μM. The increased quenching may be explained by the fact that in the absence of citrate large amount of surface stabilizing HisHA ligands form complexes with Cu^{2+}-ions in the dispersion medium and for the lack of the stabilizing ligands the PL character of the clusters dramatically decreases because the stability of the clusters also decreases. In the presence of citrate, the citrate molecules will act as the surface stabilizing molecules, so the rate of the quenching is lower.

3.4. Interpretation of the PL quenching mechanism

Detailed fluorescence studies have been performed for Cu^2 -(fluorescence quenching) and Zn^{2+}-(fluorescence enhancement) containing aqueous dispersion to understand the mechanisms. Firstly, the limit of detection (LOD) was determined for both His-Au CPs and HisHA-Au NCs systems. For this reason, the PL quenching studies have been performed at several concentrations in the range of 1.0 nM – 100.0 mM. For LOD determination, we used the calculation procedure of H.P. Loock and P.D. Wentzell, which is a widely cited LOD determination method in international publications [21]. The LOD for Cu^{2+} ions in the concentration range 1.0 nM – 100.0 mM was found to be 9.26 μM for His-Au CPs and 2.49 μM for HisHA-Au NCs. By analyzing the values, we can conclude that the four-fold difference can be identified for LOD values as well. To give more information about the nature of the interactions as well as to answer the question, that why copper causes the most intense quenching, the ζ-potential values of the HisHA-Au NCs were measured in the absence and the presence of metal ions and parallel the absorbance spectra of the NCs-containing aqueous dispersion are also registered (Fig. 5**.**).

As Fig. 5**A** represents the ζ-potential values of the HisHA-Au NCs[1] (ζ = -9.20 ± 0.86 mV) are shifted toward lower values in absolute terms after the addition of Co^{2+}- (ζ = -5.90 ± 1.72 mV) and Ni^{2+}- (ζ = -6.90 ± 1.14 mV) ions, while for Fe^{3+}-ions (ζ = +6.64 ± 0.84 mV) the surface charge takes on a positive value. These findings are in good agreement with the trend of the change of the electrokinetic potential values after the addition of di- and trivalent ions to a dispersed system. In these cases, the metal ions are bounded to the HisHA ligands located on the metallic surface resulting in static fluorescence quenching. In the case of static quenching non-fluorescent (dark) complexes are formed between the fluorophore (HisHA-Au NCs) on the ground state and the quencher (metal ions), and the number of fluorescent molecules is decreased in the excited state as it was confirmed previously in our work for AMP-Au NCs and Fe^{3+} [7]. In contrast for Cu^{2+}-ions the measured ζ-potential shows a higher negative value (ζ = -14.48 ± 0.84 mV), which may suggest that other interactions may occur for the addition of Cu^{2+}-ions. One explanation for the change may be that Cu^{2+}-ions remove the large amount of "soft" HisHA ligand from the surface forming complex(es) in the dispersion medium and the negatively charged citrate molecules, which present as a second adsorption layer around the metallic core, get closer to the surface providing steric stabilization. This assumption is confirmed by the fact that the pH of the dispersion (pH = 6.81) decreases to pH = 4.05 upon the addition of Cu^{2+}-ions. This is not observed for the other metal ions, only the change in pH due to dilution is measured. Besides, the lifetime measurement is also confirmed our hypothesis. After the addition of Cu^{2+}-ions, the determined lifetime components are drastically changed to T1 = 2.21 ± 0.12 ns (33.9 %), T2 = 0.26 ± 0.01 (18.7 %) and T3 = 7.14 ± 0.11 ns (47.4 %). They elongated values refers to the surface ligand transformation, where the citrate became more dominant at the metallic core surface. Thanks to this the Cu^{2+}-HisHA interaction, the *p* band transition of the oxygen-rich surface is more significant [22], which causes more longer fluorescence. To further confirm the above-mentioned proposed mechanism for the Cu^{2+}-containing system, the absorbance spectra of the dispersion were also recorded in the absence and the presence of Cu^{2+}-ions. As can be seen on Fig. 5**B** the HisHA-Au NCs do not show an absorbance band in the range of 440–840 nm, but after the addition of Cu^{2+}-ions, the appearance of a new band at λ = 720–725 nm is observed at pH = 4.05. This band definitely does not belong to the presence of free Cu^{2+}-ions, because the latter shows a maximum at 820–850 nm. To identify the new absorption band detected, we also recorded the spectrum of the pure ligand in the presence of Cu^{2+} -ions (HisHA/Cu^{2+} = 2:1 M ratio) at the same pH = 4.05. As Fig. 5**B** clearly represents a broad absorption band with a maximum at λ = 720–725 nm can be detected in the VIS range. The complexation of HisHA with several metal ions is well-known in the literature [15], and the spectral parameters of the formed complex(es) as a function of pH are published [15]. According to the results, the coordination of HisHA with Cu^{2+} starts at pH *ca.* 3–3.5 via hydroxamate-*O* donors, but as the pH is increased, the binding via the nitrogen donors becomes more and more dominant. Between pH 4.5–7 the amino-*N* and the imidazole-*N* donors coordinate in the complexes. In the absorbance spectrum the increase of the pH from pH ~ 2.0 to pH ~ 4.0 the detected absorbance band shows a shift from λ greater than 800 nm to λ ~ 720 nm. Normalized absorption bands of the HisHA-Cu^{2+} (dotted line) and HisHA-Au NCs-Cu^{2+} (continuous line) (Fig. 5**C**) clearly show the presence of the same complex in the samples, which confirms our earlier assumption about the change of the HisHA-citrate on the metallic surface, as the schematic drawings presents in Fig. 5**.** It has to mention that the citrate (which is present in the system) can bind to Cu^{2+}-ions at acidic pH forming [Cu_2cit_2] dimer complexes, but the characteristic absorbance band of this complex can be detected at 760 nm [23]. To exclude the formation of [Cu_2cit_2] complex preferred, the experiments were repeated in the absence of citrate as well. For absorbance spectrum, only the band at λ = 720–725 nm can be detected, which suggest the fact that the metal ions prefer more the HisHA ligand instead of citrate. After addition of Cu^{2+}-ions, the ζ -potential value of the HisHA-Au NCs (in the absence of citrate) was shifted from −8.99 ± 5.70 mV to + 9.61 ± 2.14, which further confirm the removal of the HisHA from the surface.

[1] For sub-nanometer sized NCs the ζ-potential cannot be interpreted. Most probable in our case the measured ζ-potential belongs to smaller NCs aggregates, which have a larger surface area.

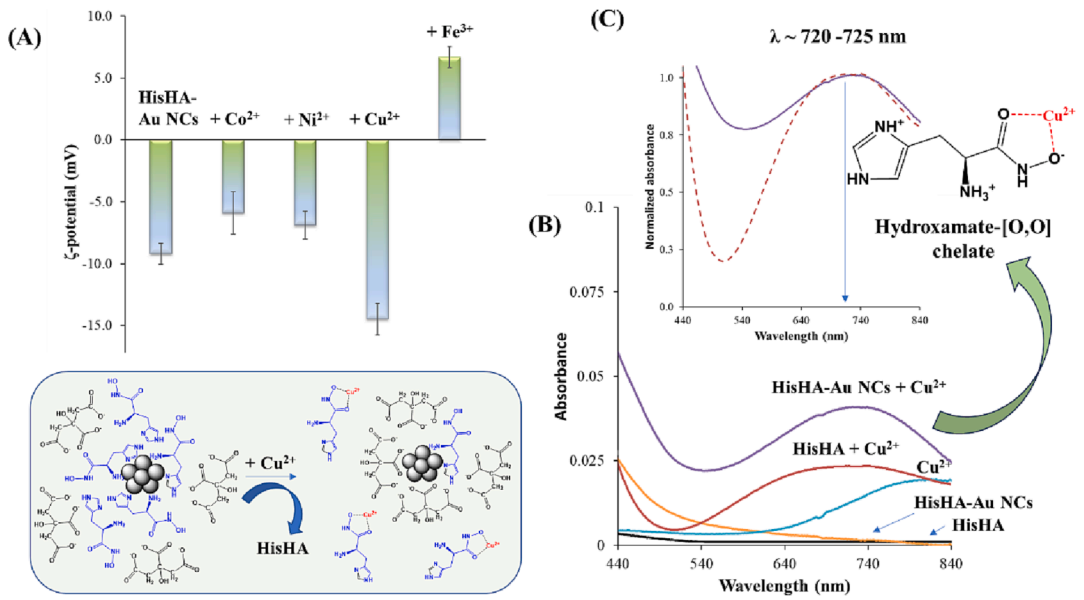

Fig. 5. **(A)** ζ-potential values of HisHA-Au NCs after addition of different metal ions ($c_{metal\ ions}$ = 1.0 mM, c_{Au} = 0.25 mM with the proposed change of the adsorption layer; **(B)** VIS spectra of the HisHA (c = 3 mM) in the absence and in the presence of Cu^{2+}-ions (c_{Cu2+} = 1.5 mM), HisHA-Au NCs (c_{Au} = 0.25 mM) in the absence and in the presence of Cu^{2+}-ions (c_{Cu2+} = 1.0 mM) and the pure Cu^{2+}-ion solution (c_{Cu2+} = 1.0 mM). **(C)** Normalized absorbance spectra of HisHA-Cu^{2+} (dotted line) and HisHA-Au NCs-Cu^{2+} (continuous line) systems with the proposed coordination mode of the complex presents in the solution at pH = 4.05.

3.5. *Interpretation of the PL enhancement mechanism*

The interaction of HisHA-Au NCs with several mono-, di- and trivalent metal ions resulted in PL enhancement only for the addition of Zn^{2+}-ions. For the detection of Zn^{2+}-ions, the fluorescence spectra of HisHA-Au NCs were recorded in the Zn^{2+} concentration range of 1 nM − 100 mM. During the measurements, the emission intensity of HisHA-Au NCs at 440 nm was determined by the addition of Zn^{2+} ions.

As Fig. 6**A** shows that the I/I_0 values follow an upward trend with a slight break depending on the added amount of Zn^{2+}-ion. Due to the

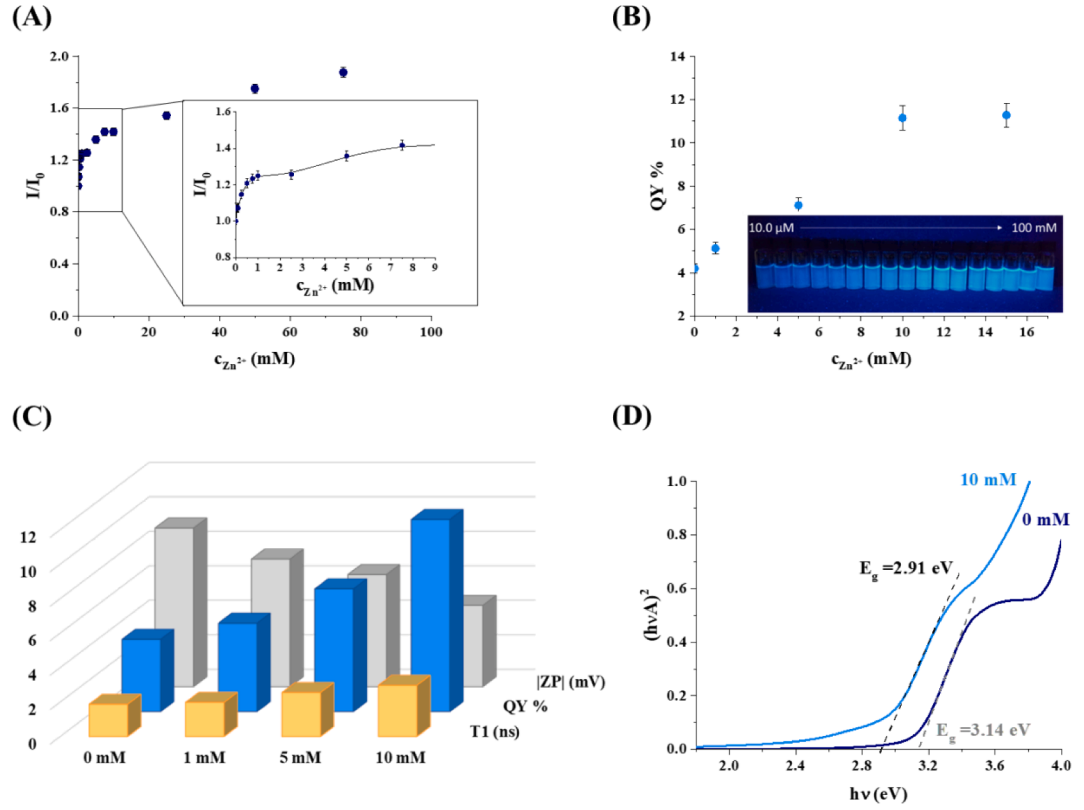

Fig. 6. **(A)**The I/I_0 values of the NCs dispersion and **(B)** the measured quantum yield % at different Zn^{2+} concentrations with the photos of the samples under UV lamp. **(C)** The measured T1, QY% and the absolute values of ζ-potential (ZP) depending on the Zn^{2+}-ion concentration. **(D)**The Tauc plot representation from the UV–Vis spectra in the case of the pure Au NCs and with 10 mM of Zn^{2+} content.

nonlinear relationship, the smallest detectable concentration (7.5 μM) was calculated by the generally accepted $LOD = 3s_{bl}/m$ equation [24], where the s_{bl} is the blank fluorescence signal without any Zn^{2+} ions, while the m is the slope of the initial range of the calibration curve. In the concentration range of 1.0 nM–5.0 μM the I/I_0 values are the same (~1.0) and the first significant enhancement starts from ~ 7.5 μM, the I/I_0 values show detectable signal in the range of 50 μM–1.0 mM (R^2 = 0.9851). Further increase in the concentration of Zn^{2+} ion causes an intense enhancement, which also causes a linear trend in the QY% between 1.0 and 10.0 mM concentrations (Fig. 6**B**). To explore the exact mechanism of the enhancement, optical and ζ-potential measurements were carried out by using different Zn^{2+} concentrations. As can be seen on Fig. 6**C**, the determined lifetime components, as well as the measured QY%, are increased with the added concentration of the Zn^{2+}-ions. In contrast, the absolute value of the ζ-potential is decreased. Based on literature data [25], the Zn^{2+} prefers the hydroxamate-[O,O] coordination through freely accessible the carbonyl oxygen and the deprotonated hydroxyl oxygen on the cluster surface. Taking into account the break of the relative fluorescence curve, it can be also concluded that the first region with slight enhancement belongs to the metal ion binding by the loosely bounded HisHA molecules near the compact structure of molecular clusters. The second region, where the larger enhancement can be detected, belongs to the non-accessible hydroxamates having freely available 'O' donors, which take part in the building of the supramolecular cluster structure. This possible Zn^{2+} binding causes a small weakening of the stability of the cluster based on the ζ-potential values. It is also well proven by the TCSPC data because the increase of the fluorescence lifetime components (**Table S1**), decisively the metal-associated components (T1 and T3), refers to the elongated fluorescence. As it is well known that the Tauc plot is a valuable method to calculate the HOMO-LUMO energy gap in the case of molecular-like metallic complexes or clusters. For this purpose, the UV–Vis spectra were recorded, where the addition of 10 mM of Zn^{2+}-ion causes large red-shift of the second absorption peak from 355 to 376 nm, which refers the change of the supramolecular structure of nanoclusters. As Fig. 6**D** presents, the initial energy gap of the Au NCs is ca. 3.1 eV, and after the Zn^{2+} ion treatment, it changed to ~ 2.9 eV, which facilitate the easier excitation of the electrons from the HOMO to LUMO bands due to the photoactive behavior of Zn^{2+}-complexes [26]. Finally, it can be concluded that the binding of Zn^{2+}-ions by the surface HisHA ligands causes a slight stability loss, but it induces a mildly elongated and significantly enhanced fluorescence.

4. Conclusion

In this work, a new biomolecule from the hydroxamic acid ligand family is presented, which shows promising results for the fabrication of Au nanoclusters functioning as metal ion sensors. On one hand, the production protocol was developed which involved the fixing of the metal ion/ligand molar ratio, metal ion concentration, pH, temperature, and reaction time. The interaction of several metal ions with the purified Au NCs stabilized by HisHA was investigated. The results suggested that Cu^{2+}-ions cause fluorescence quenching (LOD = 2.49 μM), while the PL enhancement of the NCs was obtained by Zn^{2+} (LOD = 7.5 μM). Numerous articles can be found in the literature on metal ion sensing by Au NCs, but there are a negligible number of articles that include an interpretation of the mechanisms. For both metal ions, the nature of the interaction as well as the proposed quenching and enhancing mechanisms were interpreted in detailed, where it was proved that the Cu^{2+} can remove a decisive quantity of the soft HisHA from the surface of the cluster to form complexes in the aqueous dispersion. In contrast, the Zn^{2+}-ions can form an [O,O] type bond with the hydroxamate moiety on the metallic surface, by which the QY% significantly increased (nearly 3-fold) due to the decreasing of the HOMO-LUMO energy gap.

CRediT authorship contribution statement

Gyöngyi Gombár: Methodology, Investigation, Writing – original draft. **Péter Simon:** Methodology. **Ditta Ungor:** Investigation, Writing – original draft. **István Szatmári:** Writing – review & editing. **Edit Csapó:** Conceptualization, Visualization, Writing – original draft, Writing – review & editing, Supervision, Resources.

Declaration of Competing Interest

The authors declare that they have no known competing financial interests or personal relationships that could have appeared to influence the work reported in this paper.

Data availability

Data will be made available on request.

Acknowledgement

The research was supported by the National Research, Development, and Innovation Office-NKFIH through the PD137938 and FK131446 projects. Project no. TKP2021-EGA-32 was implemented with support provided by the Ministry of Innovation and Technology (MIT) of Hungary from the National Research, Development and Innovation Fund (NRDIF), financed under the TKP2021-EGA funding scheme. Ditta Ungor thanks the financial support for the János Bolyai Research Scholarship of the Hungarian Academy of Sciences. The publication was also funded by the University of Szeged Open Access Fund (FundRef, Grant No. 6412).

Appendix A. Supplementary material

Supplementary data to this article can be found online at https://doi.org/10.1016/j.molliq.2023.122597.

References

[1] L. Zou, W. Qi, R. Huang, R. Su, M. Wang, Z. He, Green synthesis of a gold nanoparticle-nanocluster composite nanostructures using trypsin as linking and reducing agents, ACS Sustain. Chem. Eng. 1 (11) (2013) 1398–1404.
[2] Y. Zhang, C. Zhang, C. Xu, X. Wang, C. Liu, G.I.N. Waterhouse, Y. Wang, H. Yin, Ultrasmall Au nanoclusters for biomedical and biosensing applications: A mini-review, Talanta 200 (2019) 432–442.
[3] D. Ungor, K. Horváth, I. Dékány, E. Csapó, Red-emitting gold nanoclusters for rapid fluorescence sensing of tryptophan metabolites, Sensors Actuators, B Chem. 288 (2019) 728–733.
[4] R.K. Sharma, S. Gulati, S. Mehta, Preparation of gold nanoparticles using tea: A green chemistry experiment, J. Chem. Educ. 89 (2012) 1316–1318.
[5] A.V. Rane, K. Kanny, V.K. Abitha, S. Thomas, S. Thomas, Methods for Synthesis of Nanoparticles and Fabrication of Nanocomposites, Synth. Inorg. Nanomater. Adv. Key Technol. (2018) 121–139.
[6] D. Ungor, I. Dékány, E. Csapó, Reduction of Tetrachloroaurate(III) Ions With Bioligands: Role of the Thiol and Amine Functional Groups on the Structure and Optical Features of Gold Nanohybrid Systems, Nanomater. 9 (2019) 1229.
[7] D. Ungor, E. Csapó, B. Kismárton, A. Juhász, I. Dékány, Nucleotide-directed syntheses of gold nanohybrid systems with structure-dependent optical features: Selective fluorescence sensing of Fe3+ ions, Colloids Surfaces B Biointerfaces. 155 (2017) 135–141.
[8] E. Csapó, D. Ungor, Á. Juhász, G.K. Tóth, I. Dékány, Gold nanohybrid systems with tunable fluorescent feature: Interaction of cysteine and cysteine-containing peptides with gold in two- and three-dimensional systems, Colloids Surf. A Physicochem. Eng. Asp. 511 (2016) 264–271.
[9] A. Citarella, D. Moi, L. Pinzi, D. Bonanni, G. Rastelli, Hydroxamic Acid Derivatives: From Synthetic Strategies to Medicinal Chemistry Applications, ACS Omega 6 (2021) 21843–21849.
[10] J. Keth, T. Johann, H. Frey, Hydroxamic Acid: An Underrated Moiety? Marrying Bioinorganic Chemistry and Polymer Science, Biomacromolecules. 21 (2020) 2546–2556.
[11] E. Csapó, D. Ungor, Z. Kele, P. Baranyai, A. Deák, Á. Juhász, L. Janovák, I. Dékány, Influence of pH and aurate/amino acid ratios on the tuneable optical features of gold nanoparticles and nanoclusters, Colloids Surfaces A Physicochem. Eng. Asp. 532 (2017) 601–608.

[12] K. Ahlford, H. Adolfsson, Amino acid derived amides and hydroxamic acids as ligands for asymmetric transfer hydrogenation in aqueous media, Catal. Commun. 12 (12) (2011) 1118–1121.
[13] A.A. Zur, H.-C. Chien, E. Augustyn, A. Flint, N. Heeren, K. Finke, C. Hernandez, L. Hansen, S. Miller, L. Lin, K.M. Giacomini, C. Colas, A. Schlessinger, A.A. Thomas, LAT1 activity of carboxylic acid bioisosteres: Evaluation of hydroxamic acids as substrates, Bioorg. Med. Chem. Lett. 26 (20) (2016) 5000–5006.
[14] B. Kurzak, D. Kroczewska, J. Jezierska, M. Huza-Koralewicz, Stability and structure of copper(II)-L-histidinehydroxamic acid complexes, Transit. Met. Chem. 13 (4) (1988) 297–302.
[15] B. Kurzak, H. Kozłowski, E. Farkas, Hydroxamic and aminohydroxamic acids and their complexes with metal ions, Coord. Chem. Rev. 114 (2) (1992) 169–200.
[16] I.V. Mironov, E.V. Makotchenko, The hydrolysis of $AuCl_4^-$ And the stability of aquachlorohydroxocomplexes of gold(III) in aqueous solution, J. Solution Chem. 38 (2009) 725–737.
[17] J. Kimling, M. Maier, B. Okenve, V. Kotaidis, H. Ballot, A. Plech, Turkevich method for gold nanoparticle synthesis revisited, J. Phys. Chem. B. 110 (32) (2006) 15700–15707.
[18] R. Vos, Y. Engelborghs, A fluorescence study of tryptophan-histidine interactions in the peptide anantin and in solution, Photochem. Photobiol. 60 (1994) 24–32.
[19] S. Roy, A.A. Lopez, J.E. Yarnell, F.N. Castellano, Metal-Metal-to-Ligand Charge Transfer in Pt(II) Dimers Bridged by Pyridyl and Quinoline Thiols, Inorg. Chem. 61 (1) (2022) 121–130.
[20] N. Sinha, O.S. Wenger, Photoactive Metal-to-Ligand Charge Transfer Excited States in 3d6 Complexes with Cr0, MnI, FeII, and CoIII, J. Am. Chem. Soc. 145 (9) (2023) 4903–4920.
[21] H.P. Loock, P.D. Wentzell, Detection limits of chemical sensors: Applications and misapplications, Sensors Actuators B Chem. 173 (2012) 157–163.
[22] B.o. Peng, J.-F. Zhou, M. Ding, B.-Q. Shan, T. Chen, K. Zhang, Structural water molecules dominated p band intermediate states as a unified model for the origin on the photoluminescence emission of noble metal nanoclusters: from monolayer protected clusters to cage confined nanoclusters, Sci. Technol. Adv. Mater. 24 (1) (2023).
[23] D. Mastropaolo, D.A. Powers, J.A. Potenza, H.J. Schugar, Crystal Structure and Magnetic Properties of Copper Citrate Dihydrate, Cu2C6H4O7.2H2O, Inorg. Chem. 15 (1976) 1444–1449.
[24] E. Akyüz, F.B. Şen, M. Bener, K.S. Başkan, E. Tütem, R. Apak, Protein-Protected Gold Nanocluster-Based Biosensor for Determining the Prooxidant Activity of Natural Antioxidant Compounds, ACS Omega 4 (1) (2019) 2455–2462.
[25] D.A. Brown, N.J. Fitzpatrick, H. Müller-Bunz, Á.T. Ryan, Di-, tri-, and tetranuclear zinc hydroxamate complexes as structural models for the inhibition of zinc hydrolases by hydroxamic acids, Inorg. Chem. 45 (11) (2006) 4497–4507.
[26] J.A. Kübler, B. Pfund, O.S. Wenger, Zinc(II) Complexes with Triplet Charge-Transfer Excited States Enabling Energy-Transfer Catalysis, Photoinduced Electron Transfer, and Upconversion, JACS Au. 2 (10) (2022) 2367–2380.